**Proceedings of the ASME 2019 International Technical Conference and Exhibition on Packaging and Integration of Electronic and Photonic Microsystems**
**IPACK2019**
**October 7-9, 2019, Anaheim, CA, USA**

**IPACK2019-6463**

# AN EXPERIMENTAL INVESTIGATION ON THE FLUID DISTRIBUTION IN A TWO-PHASE COOLED RACK UNDER STEADY AND TRANSIENT IT LOAD

**Sadegh Khalili [1], Srikanth Rangarajan, Bahgat Sammakia**
Binghamton University-SUNY,
Binghamton, NY, USA

**Vadim Gektin**
Futurewei Technologies,
Santa Clara, CA, USA

## ABSTRACT

*Increasing power densities in data centers due to the rise of Artificial Intelligence (AI), high-performance computing (HPC) and machine learning compel engineers to develop new cooling strategies and designs for high-density data centers. Two-phase cooling is one of the promising technologies which exploits the latent heat of the fluid. This technology is much more effective in removing high heat fluxes than when using the sensible heat of fluid and requires lower coolant flow rates. The latent heat also implies more uniformity in the temperature of a heated surface. Despite the benefits of two-phase cooling, the phase change adds complexities to a system when multiple evaporators (exposed to different heat fluxes potentially) are connected to one coolant distribution unit (CDU). In this paper, a commercial pumped two-phase cooling system is investigated in a rack level. Seventeen 2-rack unit (RU) servers from two distinct models are retrofitted and deployed in the rack. The flow rate and pressure distribution across the rack are studied in various filling ratios. Also, investigated is the transient behavior of the cooling system due to a step change in the information technology (IT) load.*

Keywords: Two-phase cooling; Dielectric, Rack level cooling, Fluid distribution, HFE 7000, Heat exchanger load control

## NOMENCLATURE

| | |
|---|---|
| CDU | coolant distribution unit |
| CPU | central processing unit |
| $C_P^*$ | relative coefficient of pressure drop |
| $h$ | enthalpy, kJ/mol |
| HX | heat exchanger |
| IT | information technology |
| $P$ | pressure, kPa (psi) |
| PUE | power usage effectiveness |
| RU | rack unit |
| SWT | supply water temperature, ℃ |
| TDP | thermal design power, W |
| $\dot{V}$ | volume flow rate, lpm |

## 1. INTRODUCTION

The 2016 United States data center energy usage report [1], forecasts the data centers energy consumption will increase by 4% from 2014-2020 and reach 73 billion kWh in 2020. This is a significant shift from the 90% percent increase that was estimated for 2000-2005 and the 24% percent increase that was estimated for 2005-2010. In a recent study, Shehabi et al. [2] modeled data center energy use across the entire United States in three scenarios, namely 2020 frozen efficiency based on 2010 trend, 2020 current trends, and 2020 best practices. The frozen efficiency scenario estimates energy efficiency by considering the computational performance improvements, and the rise in demand for data center services at current trends through 2020 while holds energy efficiency practices at 2010 levels. The current trends scenario couples historical and projected equipment shipments with expected baseline improvements in equipment efficiency and operational practices from 2000 to 2020. The results estimate power usage effectiveness (PUE) of 1.9, 1.51, and 1.25 for the frozen efficiency, current trends, and best practices scenarios, respectively. This implies that energy costs in data centers can be lowered significantly by implementing best practices and the most efficient technologies.

With the ever-increasing power densities, conventional cooling techniques, such as air cooling are stretched to thermal and acoustic limitations [3]. Liquid cooling with its high heat handling capacity is an alternative to air cooling and has been on a constant lookout among thermal engineers. An IBM study [4] showed that cooling efficiency with liquid cooling can be 3500 times higher than air cooling. Liquid cooling also possesses additional benefits such as reduced noise level due to a reduced number and/or speed of server fans in liquid-cooled servers. Despite all the benefits of the single-phase liquid cooling, the risk associated with the galvanic corrosion, biological growth, and electrical conductivity of water over a long-term usage may inhibit water cooling technology in various scenarios [5].

[1] Contact author: skhalil6@binghamton.edu

Furthermore, utilizing sensible heat of the coolant leads to thermal shadowing in cold plates that are connected in series. Dielectric liquids are seen to be a potential alternative [6] to water especially with their lower viscosity and high latent heat of phase change. The merit in employing a two-phase system is also its ability to operate at a comparatively lower flow rate, and the high temperature uniformity across the chip surface [7].

Saums [8] demonstrated that the cooling capacity can be boosted by 2 and 2.5 times in an electronics system by using a pumped two-phase cooling technology compared with liquid and air-cooled solutions, respectively. Direct two-phase cooling is an emerging technology that can be deployed in data centers to cool high-density servers and racks efficiently [9]. Kulkarni et al. [5] demonstrated that two-phase cooling can be used for cooling multiple chips with cold plates that are connected in series. They successfully dissipated a total heat load of 4 kW on a single board via two separate cooling loops (2 kW per loop) using 12 serried cold plates per loop. Although there are numerous studies available on the chip scale two-phase cooling, the literature on the rack scale pumped two-phase cooling systems is limited. Valenzuela et al. [10] studied the behavior of a pumped refrigerant two-phase cooling system by considering two evaporators at different elevations to mimic a rack-scale system. The present study pertains to an air-cooled rack retrofitted with jet impingement evaporators. A coolant distribution unit (CDU) is deployed at the bottom of the rack to supply a dielectric engineered fluid (Novec HFE-7000 [11]) to the evaporators through a U-shape manifold. The boiling point of Novec-7000 is 34 °C at atmospheric pressure [11]. Temperatures, pressures and liquid flow rates are recorded at various locations to map out the flow distribution and thermal behavior of the cooling system. To the best of the authors' knowledge, this is the first full-rack scale experimental study of the performance of a direct two-phase cooling system using a dielectric.

## 2. Experimental Setup

The experimental setup includes three main parts, servers with accompanying instrumentations, a commercially available CDU, and a manifold. Seventeen 2-RU servers are deployed on the rack, which includes 16 Dell PowerEdge R530 and a Dell PowerEdge R730. Each server hosts two similar central processing units (CPU). The specification and the temperature threshold of the CPUs are listed in Table 1. Instrumentation is added to five servers at different elevations, as shown in Fig. 1. The CDU is deployed at the bottom of the rack and is responsible for supplying the coolant (Novec/HFE-7000) to the manifold via a centrifugal pump and transferring the absorbed heat in the secondary loop by the coolant to a chilled water loop from the building (primary loop) through a liquid-liquid heat exchanger (HX). The heat exchanger is connected to the reservoir directly with the intent to use the reservoir as a direct-contact condenser. A schematic of the CDU (top view), its components, and the primary and secondary cooling loops is shown in Fig. 2. A thermocouple and a pressure sensor are installed in the loops at up- and downstream of each evaporator. Additionally, a flow meter is dedicated to each evaporator loop in the instrumented servers. Also, a flow meter is installed between the pump and the manifold to measure the total flow rate supplied by the CDU. The relative location of the instrumentation with respect to evaporators A and B is shown in Fig. 2. Transparent tubing is used at the outlet of the evaporators to allow a visual inspection of the vapor quality. Two K-type thermocouples are installed in the CDU to monitor the supply and return temperatures of the coolant in the secondary loop. Also, two absolute pressure sensors with a range of 100 psi and accuracy of ± 0.5 % full scale are installed after the pump of the secondary loop and in the reservoir to monitor the supply and return pressures. Two separate centrifugal pumps are used for circulating the coolant between the reservoir and servers, and the reservoir and the HX. The intakes of the pumps are connected to the bottom of the reservoir to ensure liquid is fed to the pumps. The power consumption of the pumps is calculated by measuring voltage and current delivered to the pumps and is 250 W per pump as approximately. A manual venting valve is installed at the top of the reservoir. This valve allows extracting trapped air after filling the system.

**Table 1 Specification of the CPUs of the installed servers**

| Server | Processor (Intel Xeon) | Idle Power | TDP | Warning threshold | Critical threshold |
|---|---|---|---|---|---|
| R530 | E5-2680 v4 | 32 W | 120 W | 95 °C | 100 °C |
| R730 | E5-2687W v4 | 21 W | 160 W | 92 °C | 97 °C |

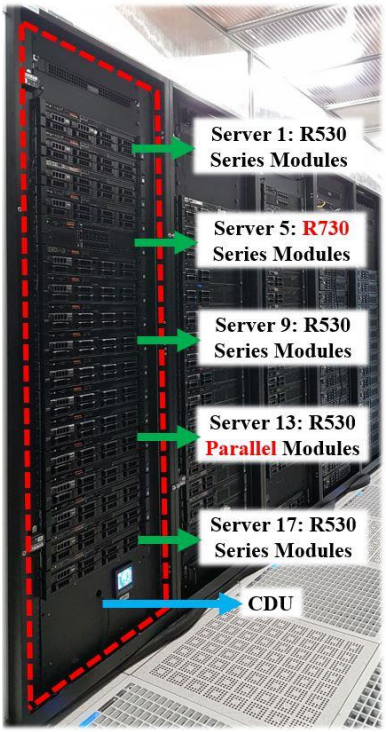


**Fig. 1 The location of the instrumented servers and the configuration of evaporators (series vs. parallel modules)**

A manifold with 32 pairs of ports is mounted vertically on the rack which distributes the coolant between the servers. Non-spill quick-connects/disconnect fittings are used which facilitate the maintenance of the servers. An adjustable differential pressure bypass valve at the top of the manifold allows controlling the pressure differential between the supply and return sides of the manifold. This spring-loaded valve bypasses the additional pressure differential created by the pump when some of the servers are disconnected. It can also be used for adjusting the supplied flow rate to the servers via changing the differential pressure between the supply and return sides of the manifold. To minimize the number of parameters impacting the flow, the bypass valve is closed in this study. Four pressure sensors are connected to the top and bottom of the supply and return sides of the manifold as shown in Fig. 2. This allows measuring $\Delta P$ along the manifold and between the supply and return sides of the manifold. The numbering system for these pressure sensors is shown on the manifold in Fig. 2.

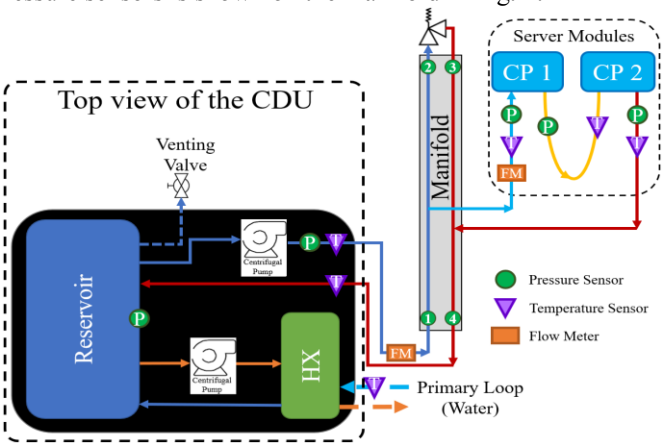


**Fig. 2 A schematic of components of the rack scale cooling system and the relative location of the instrumentation**

An R530 server is retrofitted with parallel loops with both evaporators being connected to the manifold directly with separate sets of instrumentation in each loop (server 13 in Fig. 1) while series modules are installed in the rest of the servers as shown in Fig. 2. The server loops include low gauge T-type thermocouples, Omega PX-309 pressure sensors, and Omega FPR-301 flow meters. The thermocouples are calibrated in a thermal bath with an accuracy of 0.1 °C. Thermocouple modules are built in-house to ensure effective contact between the coolant and the thermocouple's bead with minimum disruption of the flow and are added to the loop using Tee fittings. A robust bonding of the thermocouples is made to ensure zero leaks of the fluid. The range of Omega pressure sensors is 0-50 psi with a combined accuracy of ±0.25% BSL. All the pressures reported in this paper are absolute pressures. The flow meters are recalibrated with HFE-7000 for the operating range of the cooling system. An Agilent 34980A multifunction switch/ measure unit and an Omega OMB-DAQ-56 are used for recording temperatures, pressures, and flow rates. Additionally, CPU temperature and power data are collected using a Linux service [12]. The tubing between the sensors and evaporators (inside the server) is insulated to minimize heat loss between the sensors and evaporators (see Fig. 3(a)). A top-view of the CDU, and the manifold are shown in Figs. 3(b) and 3(c), respectively. This setup configuration allows a comprehensive study of the effect of server location, heat load, and evaporator module configurations on the flow distribution and cooling performance.

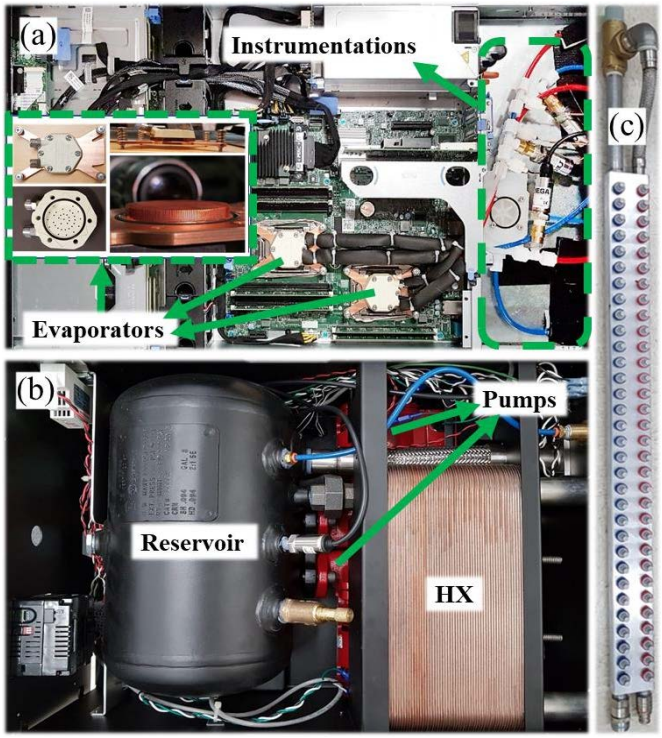


**Fig. 3 a) installed evaporators in an R530 server and the instrumentation, b) CDU (top view), c) manifold**

## 3. EXPERIMENTAL PROCEDURE

Four test cases are considered to investigate the behavior of the cooling system under various conditions. In the first (baseline) case, the flow and pressure distributions are studied without a thermal load (i.e. the servers are turned off). The results of this case provide a reference for comparison purposes. In the second case, the impact of the operating pressure on the flow distribution and thermal performance of the cooling system is investigated. In the third case, the transient behavior of the cooling system due to a step change in the CPU load of the servers is analyzed. Finally, the effectiveness of controlling supplied coolant temperature via adjusting primary loop temperature is investigated in the fourth case.

## 4. RESULTS AND DISCUSSION

### 4.1 Baseline Case

In this case, flow and pressure distributions across the rack are analyzed when servers are turned off. The supply water temperature (SWT) in the primary loop is set to 20 °C which is approximately equal to the supplied air temperature in the cold aisle. The intent is to study the flow distribution in the rack in

absence of boiling and also performing a sanity check for verifying the calibration of temperature sensors by minimizing heat losses between the coolant and air. The maximum coolant temperature difference across the evaporators A and B in the instrumented servers is 0.1 °C in this case. Figure 4 presents the flow rate through the servers across the rack. The higher flow rates through the evaporators of the server 13 are because of the parallel arrangement of the evaporators in this server, i.e. the evaporators are connected to the manifold via separate loops, while the two evaporators in the rest of the servers are connected in series imposes a higher resistance on the flow in these servers. The slight difference between flow rates in servers 1, 5, 9 and 17 in Fig. 4 can be due to the variation in the pressure drop associated with the installed instrumentation and due to the manufacturing variations of the evaporators as well as the accuracy of flow meters. The total flow rate supplied by the CDU (before the manifold) is measured as 21.36 lpm.

Figure 5 presents pressures at the bottom and top of the supply and return sides of the manifold, where locations 1 and 2 are at the bottom (inlet) and top (end) of the supply side, and locations 3 and 4 are at the top and bottom (outlet) of the return side of the manifold (see the inset schematic in Fig. 5). The pressure differentials between the top and bottom locations in the supply and return sides of the manifold are also presented in Fig. 5. These pressure differentials - $\Delta P$)1-2( and $\Delta P$)4-3) - are mainly due to the hydrostatic pressure, friction losses, and momentum changes in the manifold. Interested readers can refer to [13,14].

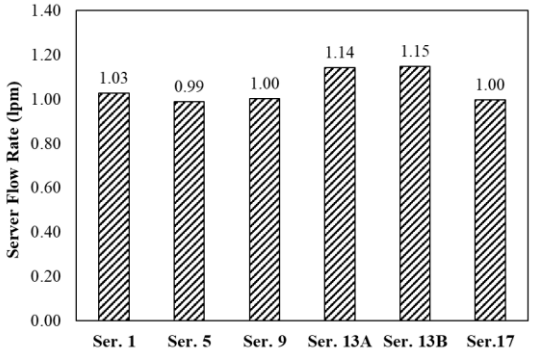


**Fig. 4 The coolant flow rate through the servers across the rack**

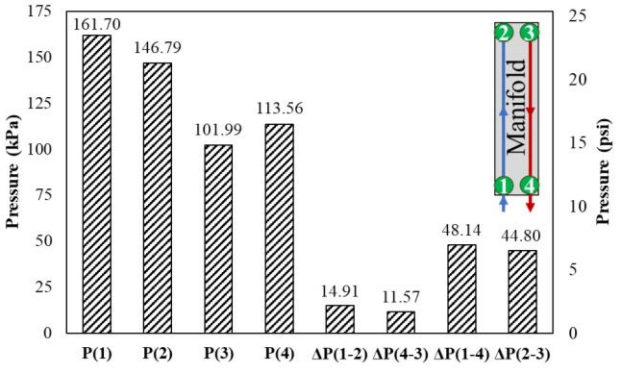


**Fig. 5 Pressure at various locations in the manifold**

Calculations show that the hydrostatic pressure between the top and bottom of the manifold is approximately 16.5 kPa (2.4 psi). Therefore, the hydrostatic pressure is the dominant term in $\Delta P$)1-2( and $\Delta P$)4-3). It should be noted that both the gravity and friction loss effects work in the same direction in the supply side of the manifold but in the opposite direction in the return side. This explains the difference between $\Delta P$)1-2( and $\Delta P$)4-3) in this case. Figure 6 presents pressure variations along the coolant loop for servers 1 and 17. The pressure drop between the pump and node 1 of the manifold is mainly due to the installed flow meter before the manifold, and dripless quick connects between the CDU and the manifold. The small pressure rise between the exit of evaporator B in server 1 and node 4 of the manifold is because of the lower elevation of node 4 compared to this server.

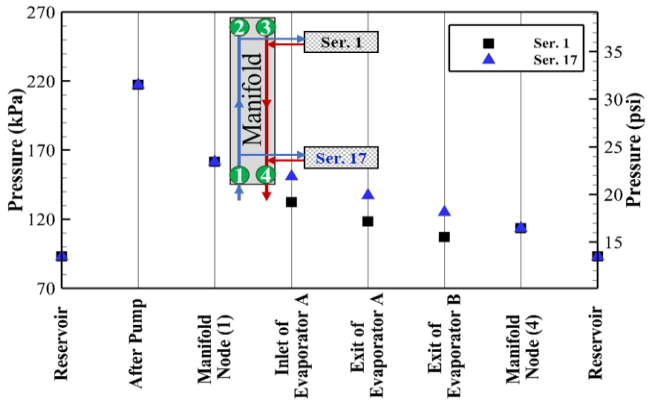


**Fig. 6 Pressure at various locations of the loop for servers 1 and 17**

### 4.2 Operating pressure case

The relation between the saturation temperature and pressure for Novec HFE-7000 is shown on a pressure-enthalpy (*p-h)* diagram in Fig. 7. The available latent heat decreases when pressure (and consequently, the saturation temperature) increases. So, the capacity of the cooling system is higher at lower pressures. However, the pressure in the system must be regulated to avoid cavitation in the pump which set a lower limit for the operating pressure of a given system. Also, the large ratio of the specific volume of vapor to the specific volume of liquid at low pressures can increase the chance of flow instabilities.

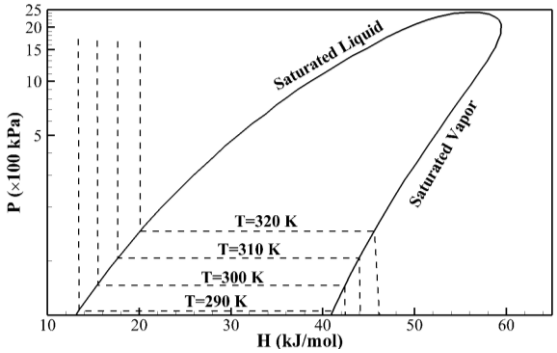


**Fig. 7 *P-h* diagram of Novec 7000 (Extracted from a 3M® datasheet)**

In a closed-loop cooling system, the overall volume of the cooling loop is constant, hence, the thermodynamic state at any

location in the of the system is a function of the specific volume of the coolant in an equilibrium. Therefore, the operating pressure at each point of the system is a function of the ratio of the initial volume of charged liquid at ambient temperature and the total volume of the cooling system (filling ratio). As mentioned earlier, the coolant pressure determines the saturation temperature at a given point, e.g. the local pressure in an evaporator determines the boiling temperature of the coolant, hence, the degree of subcooling. As a result, chip temperatures and vapor quality at the outlet of an evaporator also depend on the operating pressure of the cooling system.

In this part of the paper, the impact of the reservoir pressure on the flow distribution and the thermal performance of the cooling system is investigated when SWT is fixed at 30 ℃ and servers' CPUs are stressed fully. The reservoir pressure is adjusted by changing the filling ratio of the cooling system. Pressure in the reservoir is the lowest pressure in the loop (except at the intake of the pump) as shown in Fig. 6. At the initial stage, the system is charged under pressure to achieve the relatively high pressure of 227.5 kPa (33 psi) in the reservoir. The corresponding saturation temperature at this pressure is approximately 60℃, which means that the coolant in the reservoir is significantly subcooled. The degree of subcooling increases even further as the liquid passes the pump. After reaching a steady state, test data is collected. Next, pressure in the reservoir is reduced by extracting coolant from the loop and data is collected after the system reaches a steady state again. The pressure at various locations, flow rates, and servers' CPU temperatures are monitored to evaluate the stability of the system. Variations of the supply pressure and degree of subcooling at various locations as a function of the reservoir pressure are shown in Fig. 8. As expected, the supply pressure decreases proportionally with the reservoir pressure. Also, the degree of subcooling in the reservoir and after the pump decreases as the reservoir pressure is reduced. Although the subcooling is significant after the pump, it reduces along the coolant path as it elevates in the manifold and passes through the quick connects, tubing, and evaporators (see the degree of subcooling at the inlet of server 1 in Fig. 8).

The variation of differential pressure between the supply and return sides of the manifold at the bottom and top - $\Delta P$(1-4) and $\Delta P$(2-3), respectively - are presented in Fig. 9. While the differential pressure across the bottom of the manifold remains fairly constant, the pressure difference between nodes 2 and 3 at the top of the manifold reduces significantly after the reservoir pressure becomes less than 150.3 kPa (21.8 psi). After this point, bubbles were observed through the installed transparent tubing at the outlet of the evaporator B in servers 1 and 5. Also, the differential pressure along the return side of the manifold, $\Delta P$(4-3), drops due to the boiling. Vapor generation in the servers at the top of the rack results in a smaller mass of liquid in the return side of the manifold and consequently, decreases the hydrostatic pressure between nodes 3 and 4. The generated vapor accelerates the flow in the return manifold which also decreases $\Delta P$(4-3).

Figure 10 shows flow rates of the instrumented servers at various reservoir pressures. The maximum variation between flow rates of servers 1, 5, 9 and 17 (servers with series modules) versus the average of their flow rates is less than 2% when $P_{\text{Reservoir}}$= 227.5 kPa (33 psi). The average of flow rates in the parallel loops of server 13 is 15% higher than the average of flow rates of servers with series modules due to the smaller flow resistance in this server.

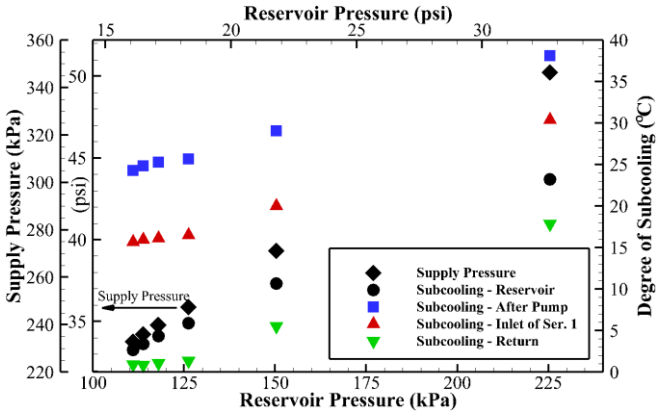


**Fig. 8 Variation of degree of subcooling in the reservoir and the supply pressure with the reservoir pressure**

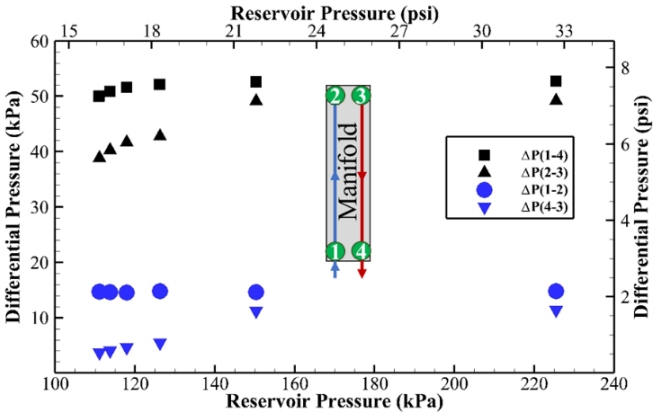


**Fig. 9 Variation of differential pressures in the manifold**

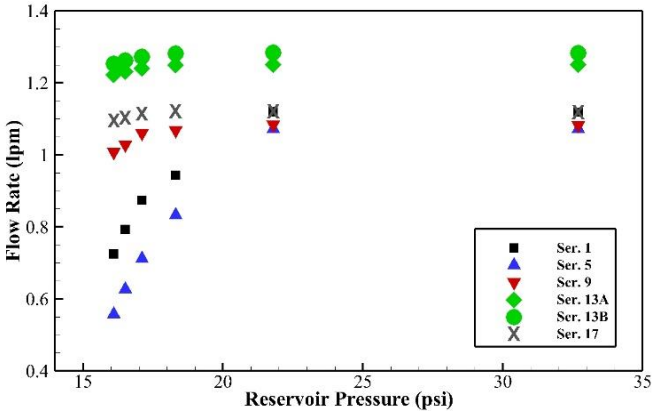


**Fig. 10 Flow rate distribution across the rack**

The uniformity of flow through the ports of the manifold depends on multiple parameters such as the ratio of the length to

the diameter of the manifold and average total head loss coefficient for the port flow [14]. In this case, a large drop is observed in the flow rate of servers 1 and 5 at lower reservoir pressures. The trend of flow rates in these servers is consistent with the trend of pressure differential at the top of the manifold shown in Fig. 9. Server 1 is located at the top of the rack, therefore, saturation temperature at the inlet of this server is lower than the rest of the servers in the rack (due to a lower gravitational head). In other words, the degree of subcooling at the inlet of this server's evaporators is lower compared to the rest of the servers. As a result, it is expected that nucleation initiates at a lower power in this server compared to other similar servers in the rack. In other words, for a given CPU power, the available capacity associated with the sensible heat is smaller, and more heat is picked up by the latent heat of the coolant in this server which translates to a higher vapor quality at the outlet of server 1. More resistance is imposed on the flow as the vapor generation rate increases which results in a lower flow rate through the evaporator. The lower flow rate, in turn, can increase the vapor quality further and trigger a continuous process in which flow rate can become dangerously low, and lead to flow instability. In fact, the relation between the heat transfer rate improvement due to boiling versus the rate of increase in the resistance on the flow is an important factor in determining the critical flow rate associated with the flow instability. To monitor this resistance change, a relative coefficient of pressure drop ($C_P^*$) is introduced as the ratio of pressure drop across a device divided by the square of the flow rate of the device at an operating point and this ratio at a reference operating point:

$$C_P^* = \left[ \frac{\Delta P}{\dot{V}} \right] / \left[ \frac{\Delta P}{\dot{V}} \right] \quad (1)$$

where $\dot{V}$ is the volume flow rate and $\Delta P$ is the differential pressure across the device. In this part, $\dot{V}$ and $\Delta P$ at the initial test of this case (when the reservoir pressure is 227.5 kPa (33 psi)) are considered as the reference values. Although $C_P^*$ does not take into account the variation of the density and viscosity of coolant with temperature, it is a valuable parameter that allows comparing pressure drop of a device under various operating conditions, and is relatively easy to measure. Figure 11 presents $C_P^*$ for the servers at various reservoir pressures. The highest $C_P^*$ is observed for server 5 followed by server 1. This is consistent with direct visual observation of authors where a higher vapor volume fraction was observed at the outlet of server 5. Although server 5 is located at a lower altitude compared to server 1, the higher power of its CPUs leads to a higher vapor generation rate. The variation of $C_P^*$ for evaporators of server 5 is presented in Fig. 12. The small variation in $C_P^*$ of evaporator A in server 5 indicates that the majority of heat is picked up by the sensible heat of the liquid. However, in evaporator B, it is seen that $C_P^*$ increases abruptly when the pressure of the system reduces. Slight vapor generation was observed at the outlet of server 9 at $P_{\text{Reservoir}}$=111 kPa (16.1 psi) while no bubble was observed at the outlet of servers 13 and 17 in this case.

It is worth mentioning that the sensitivity of the reservoir pressure to the volume of extracted coolant decreases with the filling ratio. In other words, much more liquid must be extracted in order to change the pressure in the reservoir at lower filling ratios. This is because a larger portion of the total loop volume is occupied with compressible vapor after extracting liquid.

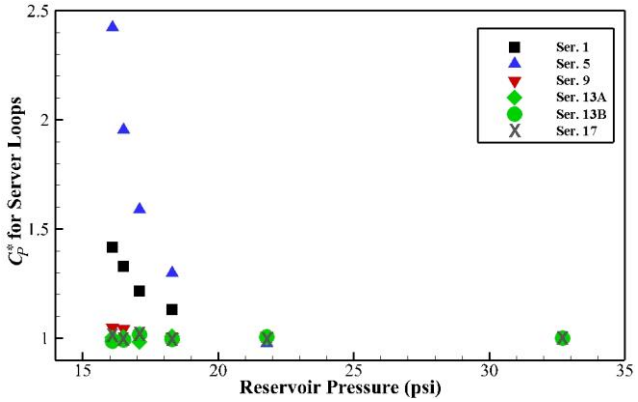


**Fig. 11 Coefficient of relative pressure drop for the instrumented servers**

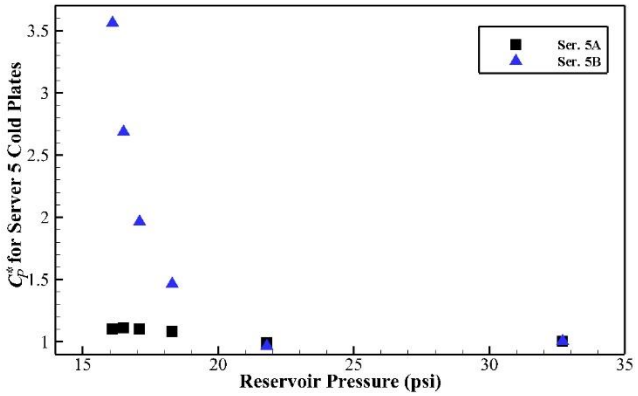


**Fig. 12 Coefficient of relative pressure drop for evaporators A and B in server 5**

Attempts to further reduce the reservoir pressure led to a continues and spontaneous decrease in the flow rate of server 5 to the point that a periodic flow oscillation in server 5 occurred when reservoir pressure reached 108.2 kPa (15.7 psi). During this oscillation, the pressure drop across evaporator A fluctuates between zero and a slightly positive value periodically and even becomes negative momentarily (which means the direction of flow through evaporator A reverses momentarily). This instability can be due to various reasons such cavitation in the pump because of a small subcooling in the reservoir, a high rate of the subsequent increase in the resistance on the flow due to a relatively high vapor generation rate, etc. As mentioned earlier, the resistance on the flow increases when the rate of vapor generation increases which can reduce the flow rate and lead to a higher vapor generation rate, which can further decrease the flow rate and lead to a no-return process. On the other hand, the increase in the volume of vapor rises the system pressure and

increases the degree of subcooling which can decrease vapor generation rate potentially and self-balance the system. Further investigations on the cause of this instability are out of the scope of this paper and authors plan to investigate this in the future.

It should be mentioned that a portion of the generated heat by a CPU is transferred to air via the PCB as shown in Fig. 13. The ratio of the heat transfer rate to the evaporator and to the PCB is a function of thermal resistance of the evaporator which depends on several factors such as vapor quality, coolant temperature, chip power, etc. Also, a portion of the heat delivered to the evaporator is transferred to air through the mounting frame and the lid of the evaporator. An accurate calculation of vapor quality at the outlet of the cold plates requires information about all the thermal resistances shown in Fig. 13, and is out of the scope of this study. However, the upper value of the vapor quality can be estimated by assuming that all the CPU power is transferred to the coolant in the form of sensible and latent heat. The sensible heat can be calculated based on the temperature measurements at the inlet and outlet of the evaporators. The rest of CPU power can be assumed to be absorbed by the latent heat of the coolant at the evaporator pressure. Following above assumptions, the vapor quality at the outlet of the evaporators A and B in server 5 at the lowest operating pressure in Fig. 12 is estimated to be 2% and 8%, respectively. It is worth mentioning that the focus of this study is on the fluid distribution and overall performance of the cooling system. Accurate thermal measurements are cumbersome in the current rack-level setup due to the inherent complexities of the setup and consequent uncertainties. Such measurements can be carried out in a well-controlled benchtop setup and is out of the focus of this paper.

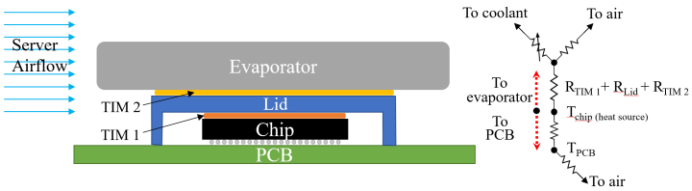


**Fig. 13 Schematic of heat transfer paths from the chip**

### 4.3 Transient behavior of the cooling system

As mentioned earlier, the workload in many data centers exhibits periodic patterns (daily or weekly) [12,15–19]. A change in the workload affects the heat load on cooling systems and consequently, can change the operating conditions of a two-phase cooling system. In this section, the transient behavior of the cooling system due to a step change in the heat load is studied. In this case, SWT is fixed at 30 °C and the servers operate in idle mode initially. After 60 seconds, CPUs of all the servers are stressed fully to mimic a sudden change in the heat load. Temperatures, pressures and flow rates are collected until the system reaches a steady state again. The variation of CPU temperatures, flow rates and pressures at various locations are monitored to assess the systems' conditions. Figure 14 presents the variation of pressure in the manifold during the test. It is observed that the manifold pressures rise with time. Similarly, the supply and reservoir pressures increase as shown in Fig. 15. This pressure rise is due to the expansion of the coolant as a result of an overall rise in its temperature (see temperatures in Fig. 15) and the vapor generation in evaporators while the total volume of the system is constant. The temperature rise is due to the increase in the heat carried by the cooling system. This increases the temperature at the outlet of HX while the SWT is fixed which increases the reservoir temperature and supply temperature subsequently.

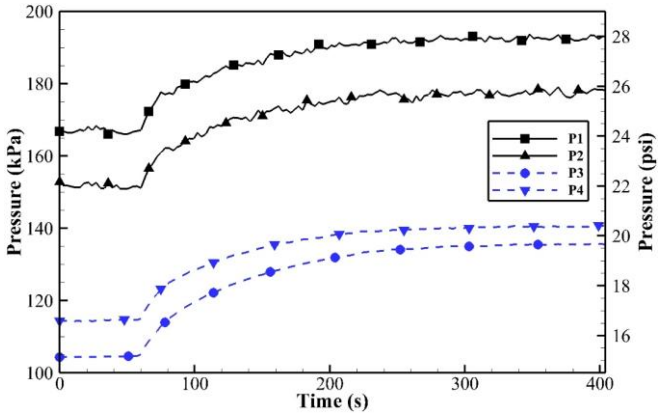


**Fig. 14 Pressure at various locations inside the manifold**

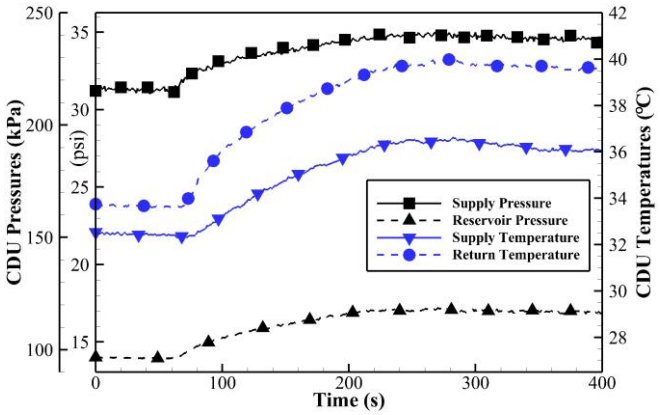


**Fig. 15 Pressure and temperature data of CDU**

Figure 16 shows that the pressure differential between the supply and return sides at the top of the manifold - $\Delta P$(2-3) - reduces with time. Simultaneously, the differential pressure between the top and bottom of the return manifold - $\Delta P$(4-3) - decreases which is due to the vapor generation in the servers at the top of the rack. Figure 17 demonstrates the presence of boiling in loops of servers 1 and 5. Visual inspections at the end of the experiment confirmed the vapor generation at the outlet of servers 1 and 5. This figure also reveals a slight boiling in the evaporators of server 9 while authors were not able to visually verify it, potentially due to the size and concentrations of bubbles or bubble collapsing as a result of the subcooling. It is worth repeating that $C_P^*$ is defined in this paper to observe the variation of the resistance on the flow associated with boiling in evaporators, and the impact of the change in coolant properties is not included in the definition.

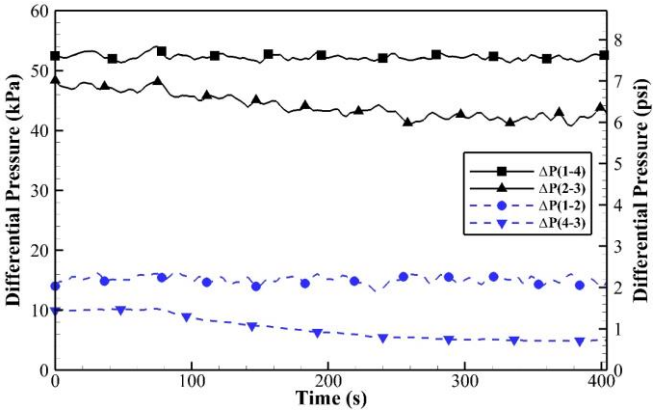


**Fig. 16 Variation of differential pressures in the manifold**

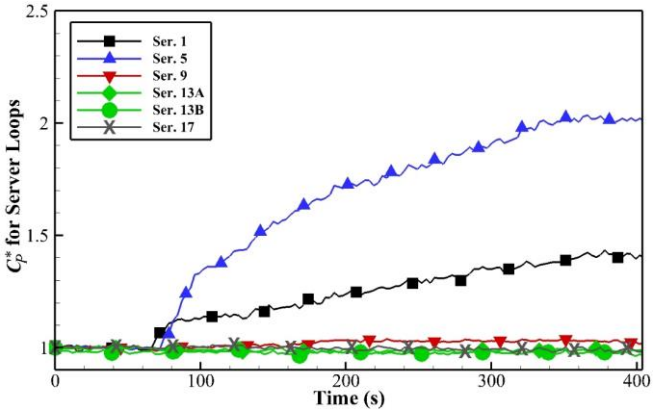


**Fig. 17 Coefficient of relative pressure drop for the servers**

The change in the viscosity due to the rise in liquid temperature in evaporator A - where no boiling is observed - and the initiation of boiling in the evaporator B have opposite effects on the server's flow rate. As demonstrated in Fig. 18, flow rates of servers 1 and 5 gradually decrease after stressing CPUs. Also, a slight decrease in the flow rate of server 9 is observed while no significant change is seen in the flow rate of the rest of the servers. Therefore, it is perceived that the increase in resistance on the flow due to boiling has the dominant role compared to the effect of liquid's viscosity change. Again, the lower flow rate of server 1 compared to other servers with a similar configuration (servers 9 and 17) demonstrates the importance of gravitational head of liquid on the cooling of servers at different elevations. For example, calculations showed that the hydrostatic pressure due to the column of liquid coolant in the installed manifold is 15.8 kPa (2.3 psi) in this case. This hydrostatic pressure alters the saturation temperature of the coolant between 2.3 to 3.5 °C for operating pressures of 220.6 to 131 kPa (32 to 19 psi), respectively. This change in the hydrostatic pressure can be neutralized by installing a custom designed manifold.

Table 2 compares CPU temperatures of the instrumented servers at the initial steady state (no CPU load) and the final steady state (100% CPU load). The conductivity, thickness, and uniformity of the used thermal interface material (TIM) between the evaporators and the CPU can influence a package temperature. Also, the authors did not calibrate the CPUs' built-in temperature sensors and the decimals in Table 2 are only for limiting the uncertainty in $\Delta T$ calculations. However, this data still can be used for qualitative observations. An interesting observation is that the temperatures of the CPUs in server 5 at the initial steady state are lower than the temperature of the supplied coolant (see the coolant temperature in Fig. 15). The cold aisle air temperature was set to 20 °C in all the tests which is lower than the supplied coolant temperature in this case. The lower idling temperature of CPUs in this server compared to the rest of the servers is thought to be due to the low idling power of the CPUs (see Table 1) and the larger CPU package dimensions in this server. The larger package size increases the heat transfer rate to air through the mainboard of this server and results in a lower chip temperature. Therefore, at high SWTs, an undesirable heat transfer from the supplied coolant to air can be present in servers that are powered off, idling, or operate at a low CPU utilization. In other words, the higher temperature of coolant compared to the CPU temperature causes a reverse heat transfer from the liquid to air through the CPUs. This can add extra thermal load on the air-cooling units in a data center. Therefore, the temperature of the supplied coolant should be chosen wisely.

Authors were able to operate the rack under full load at SWT = 49 °C while the maximum temperature of CPUs in the rack did not exceed 85 °C. However, higher server fan speeds were observed due to a higher CPU temperature. Also, the heat transfer to the environment was found significant at this SWT because of a lack of insulation for the tubing between the servers and the manifold, and around the manifold's frame.

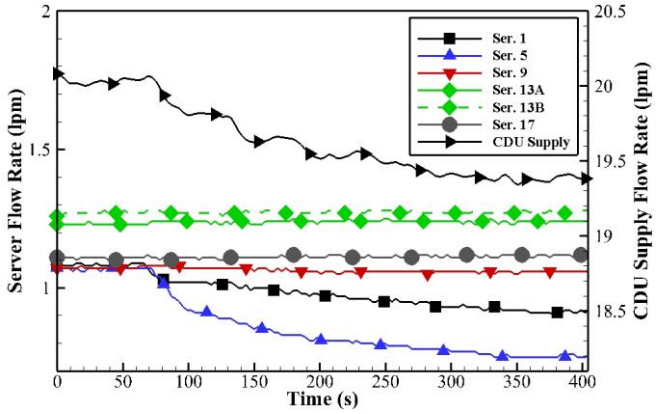


**Fig. 18 The flow rate of the CDU and the instrumented servers**

As shown in Fig. 6, the coolant's pressure drops as it passes through each evaporator in a series module configuration. As a result, the saturation temperature of the coolant in evaporator B is lower than the saturation temperature in evaporator A (due to the lower coolant pressure) which can lead to a lower temperature of the later CPU in a two-phase cooling loop. This is consistent with CPU temperatures shown in Table 2 where CPU B is cooler compared to CPU A in server 5, and $\Delta T_{CPU}$ is smaller for servers at higher elevations (where boiling is observed). The higher temperature of $CPU_B$ in servers 1, 9, and

17 is because of thermal shadowing due to the fact that a large portion of heat in these servers are picked up by the sensible heat of the coolant as a result of the lower CPU power in these servers. It is worth repeating that the evaporators in server 13 are connected to the manifold via separate loops, therefore, the CPU temperatures are expected to be similar.

**Table 2: Temperature of CPUs before and after stressing CPUs**

| Ser. # | Initial Steady State | | | Final Steady State | | |
|---|---|---|---|---|---|---|
| | $T_{CPU\,A}$ | $T_{CPU\,B}$ | $\Delta T_{CPU}$ | $T_{CPU\,A}$ | $T_{CPU\,B}$ | $\Delta T_{CPU}$ |
| Ser. 1 | 31.1 ℃ | 31.9 ℃ | 0.8 ℃ | 59.6 ℃ | 59.8 ℃ | 0.2 ℃ |
| Ser. 5 | 28.1 ℃ | 27.9 ℃ | -0.2 ℃ | 70.8 ℃ | 66.7 ℃ | -4.1 ℃ |
| Ser. 9 | 30.4 ℃ | 31.8 ℃ | 1.4 ℃ | 58.7 ℃ | 59.4 ℃ | 0.7 ℃ |
| Ser. 13 | 30.2 ℃ | 30.8 ℃ | 0.6 ℃ | 57.6 ℃ | 57.8 ℃ | 0.2 ℃ |
| Ser. 17 | 31 ℃ | 32.1 ℃ | 1.1 ℃ | 60.2 ℃ | 62.3 ℃ | 2.1 ℃ |

### 4.4 Controlling Supply Water Temperature

In case 4.3, it was observed that a change in the heat load can shift the operating conditions of the cooling system when the primary loop temperature was fixed. The primary loop temperature (SWT) can be adjusted to decrease the impact of heat load variation on the supplied coolant conditions. In other words, SWT can be controlled to achieve a fixed coolant supply temperature (or pressure) in the CDU. In this part of the paper, a control system is designed for this purpose and implemented. The control system adjusts the primary loop temperature (SWT) based on an error signal and the rate of change in the error signal. The error signal is defined as the difference between the current temperature of the supplied coolant and a desired setpoint. The control system allows a tolerance of 0.3℃ between the setpoint and current temperature. To investigate the impact of the control system on the cooling system, the experimental procedure in case 4.3 is repeated when the desired supply coolant temperature setpoint is set to 32.5 ℃. The CDU data in Fig. 19 demonstrates a successful implementation of the control system where the control system brings the temperature of the supplied coolant back to the desired setpoint by adjusting SWT. Although the supply temperature is brought back to the initial temperature, the supply and reservoir pressures at the final steady state are higher than the corresponding pressures at the initial steady state with no IT load. This is due to an overall rise in the loop pressure as a result of vapor generation. However, compared to case 4.3, the overall system pressure is slightly lower (see Fig. 15) which can potentially decrease the degree of subcooling. This, in turn, can result in a higher vapor generation rate in the evaporators because of the reduced available sensible heat of the coolant. This higher vapor generation rate increases the flow resistance which can decrease the flow rate through the evaporators. Table 3 compares flow rates for the servers and the CDU in the final steady state in the absence and presence of the control system (cases 4.3 and 4.4, respectively). It is observed that flow rates of servers 1 and 5 in case 4.4 are lower compared to case 4.3. Flow rates of servers 13 and 17 are slightly lower than case 4.3 which is due to the smaller differential pressure between the supply and return sides of the manifold in case 4.4. Overall, it is observed that implementing the control system can decrease subcooling but affects the flow rate of the servers in this cooling system.

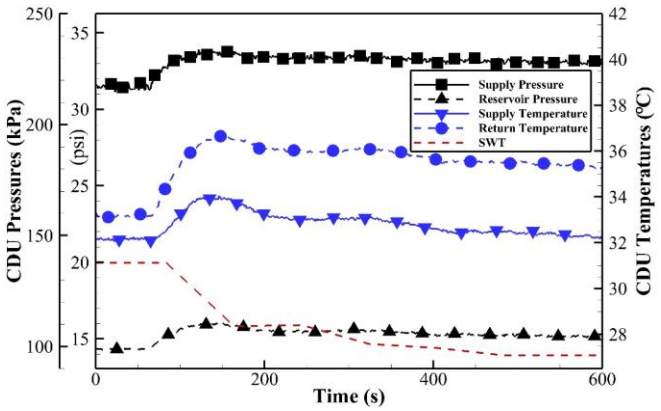


**Fig. 19 Pressure and temperature data of CDU**

**Table 3: Comparison of flow rates in cases 4.3 and 4.4 in the final steady state (flow rates in lpm)**

| Case # | Ser. 1 | Ser. 5 | Ser. 9 | Ser.13A | Ser.13B | Ser. 17 | CDU |
|---|---|---|---|---|---|---|---|
| Case 4.3 | 0.92 | 0.75 | 1.06 | 1.24 | 1.27 | 1.12 | 19.39 |
| Case 4.4 | 0.79 | 0.59 | 1.03 | 1.20 | 1.23 | 1.05 | 19.32 |

## 5. Conclusions

In this paper, a commercial pumped two-phase cooling system is investigated in a full rack level. The experiments demonstrated a simultaneous cooling of multiple servers with different heat dissipation loads at different elevations and different evaporator loop configurations (series/parallel modules). Special attention is given to the parameters that can affect the flow distribution across the rack. A non-dimensional coefficient ($C_P^*$) is defined to monitor the state of boiling in the evaporators. The major outcomes of this study are as follows:

1. Subcooling is inevitable in a typical pumped cooling system due to the inherent pressure rise in the pump which increases the saturation temperature of the coolant. However, the magnitude of subcooling can be minimized by understanding the behavior of the system and a proper choice and sizing of components based on the expected heat load on the system.
2. The impact of the hydrostatic pressure on the flow distribution is found to be significant. This pressure can alter the degree of subcooling at the inlet of servers across the rack, hence, servers at higher elevations experience a higher vapor generation rate at a given heat load. This can affect the uniformity of flow delivery across the rack significantly, e.g. the flow rate through servers at higher elevations can be significantly lower than the servers at lower elevations. A properly designed manifold can decrease the impact of hydrostatic pressure and help achieving a more uniform flow distribution. The authors suggest placing the high-power equipment at lower elevations in a heterogenous rack. Closed loop two-phase cooling devices confined within the servers' chassis can be an alternative solution in which the impact of the hydrostatic pressure is eliminated.

3. A change in the heat load on a two-phase cooling system can shift the operating conditions of the system when the SWT is fixed. This shift can affect the thermal performance and flow distribution across the rack by changing the saturation temperature of the coolant. A control system is designed to control the temperature of the supplied coolant via adjusting SWT and tested experimentally in this paper. Results showed that the impact of the heat load on the operating conditions of the cooling system can be reduced but cannot be eliminated entirely by implementing this control system. Alternatively, controlling coolant supply pressure (not tested in this paper) via adjusting SWT can be implemented. Also, a thermal expansion tank can be connected to the loop to absorb pressure changes. Further experimental testing is required to provide more insight on the operating limits, stability, and reliability of a pressure-controlled control system.
4. An undesirable heat transfer from the coolant into idling chips and subsequently, into the cooling air can be present at high supply coolant temperatures. This can add a thermal load on the air-cooling systems in data centers. Further investigations are required to evaluate the benefits of a higher SWT versus a potential added load on the air-cooling units due to this heat transfer in a data center room.

It should be mentioned that some of the behaviors observed in this paper are due to the architecture of the cooling loop in the tested system, e.g. the configuration of the heat exchanger in the loop. Hence, the results may not be generalizable to cooling systems with different two-phase loop architecture. Authors think there is significant room for improving the existing design via optimizing the design of manifold and evaporators, proper sizing of the components based on the expected heat load, implementing a sophisticated control system, etc. Further investigations should pave the way for a better understanding and utilization of the pumped two-phase flow in cooling server racks.

## ACKNOWLEDGMENTS

The authors would like to thank Dr. Husam Alissa from Microsoft, and Prof. Kanad Ghose, Anuroop Desu and Kevin D. Hall from Binghamton University computer science department and Data Center Group. We would also like to thank the ES2 partner universities for their support and advice. This work is supported by NSF IUCRC Award No. IIP-1738793 and MRI Award No. CNS1040666.

## REFERENCES

[1] Shehabi, A., Smith, S., Sartor, D., Brown, R., Herrlin, M., Koomey, J., Masanet, E., and Lintner, W., 2016, *United States Data Center Energy Usage Report*.

[2] Shehabi, A., Smith, S. J., Masanet, E., and Koomey, J., 2018, "Data Center Growth in the United States: Decoupling the Demand for Services from Electricity Use," Environ. Res. Lett., **13**(12).

[3] Kadam, S. T., and Kumar, R., 2014, "Twenty First Century Cooling Solution: Microchannel Heat Sinks," Int. J. Therm. Sci., **85**, pp. 73–92.

[4] Schmidt, R., 2009, "Packaging of New Servers - Energy Efficiency Aspects," *1st Berkeley Symposium on Energy Efficient Electronics*.

[5] Kulkarni, D., Tang, X., Ahuja, S., Dischler, R., and Mahajan, R., 2018, "Experimental Study of Two-Phase Cooling to Enable Large-Scale System Computing Performance," Proc. 17th Intersoc. Conf. Therm. Thermomechanical Phenom. Electron. Syst. ITherm 2018, pp. 596–601.

[6] Hetsroni, G., Mosyak, A., Segal, Z., and Ziskind, G., 2002, "A Uniform Temperature Heat Sink for Cooling of Electronic Devices," Int. J. Heat Mass Transf., **45**(16), pp. 3275–3286.

[7] Mudawar, I., and Wadsworth, D. C., 1991, "Critical Heat Flux from a Simulated Chip to a Confined Rectangular Impinging Jet of Dielectric Liquid," Int. J. Heat Mass Transf., **34**(6), pp. 465–1479.

[8] Saums, D. L., 2010, "Vaporizable Dielectric Fluid Cooling for IGBT Power Semiconductors," *2010 6th Int. Conf. Integrated Power Electron. Syst.*, pp. 1–7.

[9] Capozzoli, A., and Primiceri, G., 2015, "Cooling Systems in Data Centers: State of Art and Emerging Technologies," Energy Procedia, **83**, pp. 484–493.

[10] Valenzuela, F., Ortega, A., Jones, G., Fleischer, A., Schon, S., and Tipton, R., 2017, "Experiments on the Simultaneous Two-Phase Liquid Cooling of Multiple Simulated Servers at Differing Vertical Rack Positions in Steady State," *16th IEEE Intersoc. Conf. Therm. Thermomechanical Phenom. Electron. Syst. (ITherm) 2017*, pp. 871–877.

[11] "3M™ Novec™ 7000 Engineered Fluid" [Online]. Available: https://multimedia.3m.com/mws/media/121372O/3m-novec-7000-engineered-fluid-tds.pdf.

[12] Stachecki, T. J., and Ghose, K., 2015, "Short-Term Load Prediction and Energy-Aware Load Balancing for Data Centers Serving Online Requests*," *42nd International Symposium on Computer Architecture (ISCA), Portland, OR, June*, pp. 13–17.

[13] Kayahan, E., Eroglu, I., and Koku, H., 2016, "Design of an Outdoor Stacked – Tubular Reactor for Biological Hydrogen Production," Int. J. Hydrogen Energy, **41**(42), pp. 19357–19366.

[14] Wang, J., 2011, "Theory of Flow Distribution in Manifolds," Chem. Eng. J., **168**(3), pp. 1331–1345.

[15] Gmach, D., Rolia, J., Cherkasova, L., and Kemper, A., 2009, "Resource Pool Management: Reactive versus Proactive or Let's Be Friends," Comput. Networks, **53**(17), pp. 2905–2922.

[16] Arlitt, M., and Jin, T., 2000, "A Workload Characterization Study of the 1998 World Cup Web Site," IEEE Netw., **14**(3), pp. 30–37.

 

[17] Gandhi, A., 2013, “Dynamic Server Provisioning for Data Center Power Management,” Carnegie Mellon University.
[18] Atikoglu, B., Xu, Y., Frachtenberg, E., Jiang, S., and Paleczny, M., 2012, “Workload Analysis of a Large-Scale Key-Value Store,” *ACM SIGMETRICS Performance Evaluation Review*, ACM, pp. 53–64.
[19] Khalili, S., Mohsenian, G., Desu, A., Ghose, K., and Sammakia, B., 2019, “Airflow Management Using Active Air Dampers in Presence of a Dynamic Workload in Data Centers,” *2019 35th Thermal Measurement, Modeling & Management Symposium (SEMI-THERM)*, San Jose, CA, p. Under publish.